DOI: 10.1002/ejic.200800069

Metal Halide/N-Donor Organic Ligand Hybrid Materials with Confined Energy Gaps and Emissions

Wei Wang,[a] Juan Qiao,*[a] Guifang Dong,[a] Liduo Wang,[a] Lian Duan,[a] Deqiang Zhang,[a] and Yong Qiu*[a]

Keywords: Organic–inorganic hybrid composites / Halides / Luminescence

Four group 12 metal halide/N-donor organic ligand hybrid materials, $ZnCl_2(AEC)_2$ (**1**), $ZnI_2(AEC)_2$ (**2**), $CdI_2(AEC)_2$ (**3**), and $HgI_2(AEC)_2$ (**4**) [AEC=N-(2-aminoethyl)carbazole] were synthesized and characterized. Single crystals of $ZnCl_2(AEC)_2{\cdot}CH_3CN$ (**1**·CH_3CN) and $ZnI_2(AEC)_2{\cdot}CH_3CN$ (**2**·CH_3CN) were obtained from solutions. Single-crystal X-ray diffraction analysis revealed that **1**·CH_3CN and **2**·CH_3CN form quasi-1D structures of $(ZnCl_2)_n$ and $(ZnI_2)_n$ chains. The two AEC ligands in one hybrid molecule are dissymmetric due to the steric hindrance effect of the AEC moiety and the hydrogen bonding of the CH_3CN guest molecules. The UV/Vis spectra of compounds **1**–**4** were measured, and the optical energy gaps (E_g) of compounds **1**–**3** are very close to that of AEC; the value of E_g for compound **4** is a little smaller. Steady and transient photoluminescence studies revealed that the emissions of compounds **1**–**3** are attributed to the AEC ligands, whereas compound **4** does not emit light owing to the heavy-atom effect. Theoretical studies of the electronic structures confirmed that the optical energy gaps and emissions of the hybrid materials are almost confined by the AEC organic ligand rather than the metal halides.

(© Wiley-VCH Verlag GmbH & Co. KGaA, 69451 Weinheim, Germany, 2008)

Introduction

Organic–inorganic hybrid materials based on metal halides and organic N-donor ligands have drawn much attention because of their tunable crystal structures[1] and optical properties.[2] The organic ligands (amines or nitrogen-heterocyclic compounds) play an important role in hybrid systems, as they have tremendous configurations and different numbers of the coordinate sites[3] that affect the crystal structures and properties. Generally, hybrid materials containing π-conjugated organic ligands are photoluminescent,[4] but most of the organic ligands used have large energy gaps and poor charge-transport properties.[5] As a result, the energy gaps of the hybrid materials are mainly tuned by the inorganic metal halides, and the emission spectra of the hybrid materials are also changed with different metal halides.[6]

Herein, we chose *N*-(2-aminoethyl)carbazole (AEC) as the organic ligand, because the carbazole ring is considered to be a good charge-transport group[7] and some new properties can be anticipated by introducing the AEC ligand into organic–inorganic hybrid systems. We obtained a new type of hybrid material, namely, $ZnCl_2(AEC)_2$ (**1**), $ZnI_2(AEC)_2$ (**2**), $CdI_2(AEC)_2$ (**3**), and $HgI_2(AEC)_2$ (**4**). The crystal structures of **1**·CH_3CN and **2**·CH_3CN were determined and both have quasi-1D structures of $(ZnCl_2)_n$ and $(ZnI_2)_n$ chains. The UV/Vis spectra, IR, transient photoluminescence, and emission spectra of **1**–**4** were measured. The results reveal that the energy gaps and emissions of these hybrid materials are more likely to be determined by the organic AEC ligand instead of the metal halides. Molecular orbital calculations were also performed to investigate the emission mechanisms of these hybrid materials.

[a] Key Lab of Organic Optoelectronics & Molecular Engineering of Ministry of Education, Tsinghua University
Tsinghua Yuan Street No. 1, 100084 Beijing, China
Fax: +86-10-62795137
E-mail: qiuy@mail.tsinghua.edu.cn
qjuan@mail.tsinghua.edu.cn

Results and Discussion

Synthesis of Hybrid Materials 1–4

The synthesis of compounds **1**–**4** is outlined in Scheme 1. The AEC ligand was prepared by a phase-transfer catalysis reaction,[8] and the product was purified by vacuum sublimation. $ZnCl_2$, ZnI_2, CdI_2, and HgI_2 were treated with AEC in a 1:2 ratio in acetonitrile. Single crystals of $ZnCl_2(AEC)_2{\cdot}CH_3CN$ (**1**·CH_3CN) and $ZnI_2(AEC)_2{\cdot}$

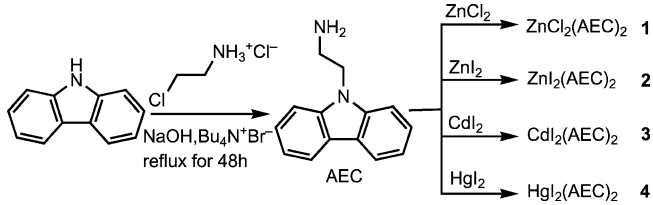

Scheme 1. Synthesis of the hybrid materials and their labels.

 © 2008 Wiley-VCH Verlag GmbH & Co. KGaA, Weinheim

CH_3CN (**2**·CH_3CN) were obtained by slow evaporation from the acetonitrile solutions with uncoordinated guest CH_3CN molecules. Both compounds crystallize in the monoclinic $P2_1/n$ space group. The powder samples of **1**–**4** do not contain guest CH_3CN molecules after being dried in vacuo.

Crystal Structures of 1·CH_3CN and 2·CH_3CN

Compounds **1**·CH_3CN and **2**·CH_3CN were analyzed by single-crystal X-ray diffraction. Selected bond lengths and angles are listed in Table 1. The perspective drawings of **1**·CH_3CN and **2**·CH_3CN are shown in Figure 1. Packings of the molecules are shown in Figure 2. Typically, hybrid systems consisting of metal halides and organic N-donor ligands that are small, such as pyridine, belong to the C_{2v} point group.[9] Xiao et al.[10] found that for the relatively large ligand 1,1′-(1,5-pentanediyl)bis-1*H*-benzimidazole (pbbm), there was no symmetric plane for the hybrid $\{[ZnCl_2(pbbm)]\cdot(H_2O)_{1/8}\}_n$, which had a 1D helical structure. Compounds **1** and **2** belong to the C_1 point group, and the absence of symmetric planes in the molecules also indicate the steric hindrance caused by the AEC ligand. Hydrogen bonding of the guest CH_3CN molecules may also cause distortion in the crystal structures of compounds **1** and **2**.

Table 1. Selected bond lengths [Å] and angles [°] for **1**·CH_3CN and **2**·CH_3CN.

	1·CH_3CN		
C1–C2	1.396 (4)	C1–N2	1.384 (4)
C25–C26	1.519 (4)	C26–N1	1.468 (3)
Zn1–Cl1	2.235 (1)	Zn1–Cl2	2.266 (1)
Zn1–N1	2.022 (2)	Zn1–N3	2.031 (2)
C1–C2–C3	117.1 (4)	C25–C26–N1	114.0 (2)
Cl1–Zn1–Cl2	107.9 (1)	N1–Zn1–N3	108.3 (1)
Cl1–Zn1–N3	110.3 (1)	Cl1–Zn1–N1	112.1 (2)
	2·CH_3CN		
C1–C2	1.394 (7)	C1–N2	1.389 (6)
C25–C26	1.518 (6)	C26–N1	1.476 (5)
Zn1–I1	2.582 (1)	Zn1–I2	2.604 (1)
Zn1–N1	2.050 (4)	Zn1–N3	2.030 (4)
C1–C2–C3	116.8 (5)	C25–C26–N1	114.2 (4)
I1–Zn1–I2	111.7 (1)	N1–Zn1–N3	111.0 (2)
I1–Zn1–N3	108.5 (2)	I2–Zn1–N3	107.4 (1)

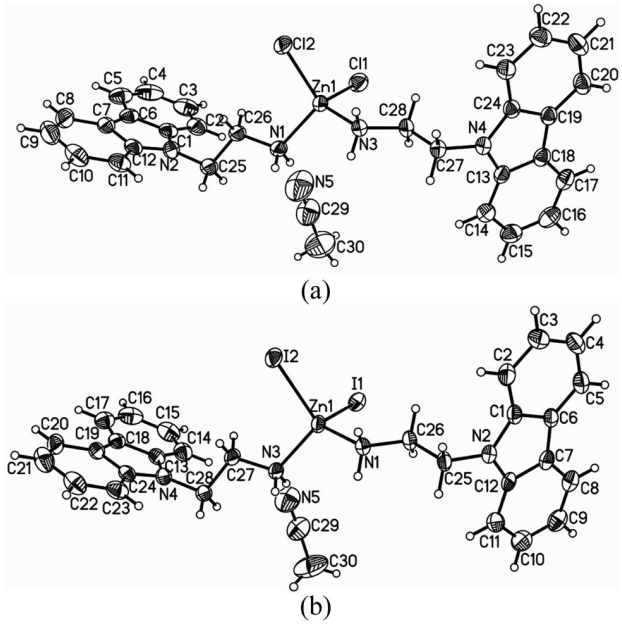

Figure 1. ORTEP drawings of compounds **1**·CH_3CN (a) and **2**·CH_3CN (b) with 30% probability ellipsoids.

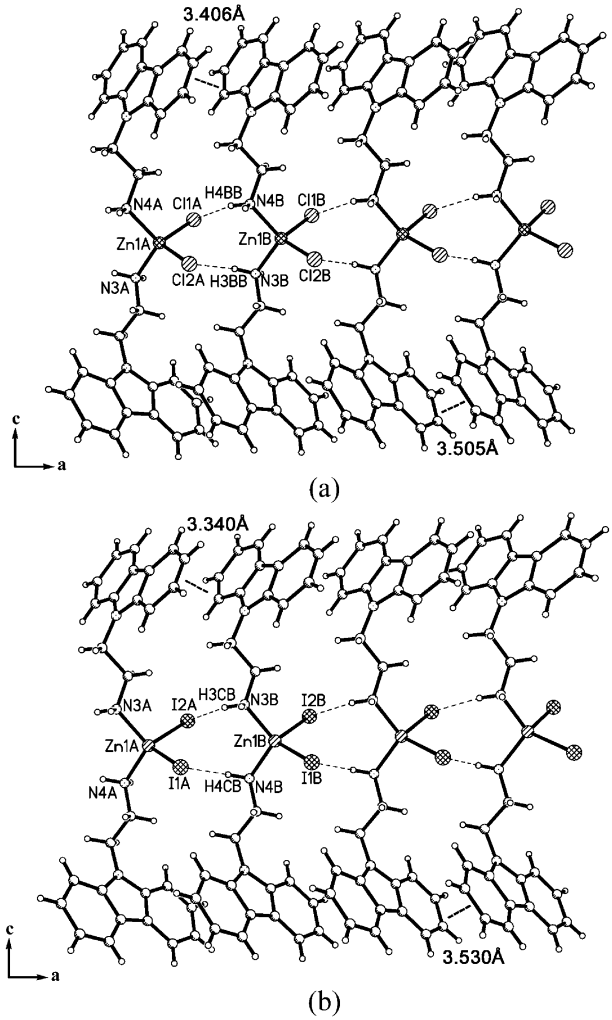

Figure 2. Hydrogen bonds and π–π stacking in compounds **1** (a) and **2** (b) (guest CH_3CN molecules are omitted for clarity); thin dashed lines represent hydrogen bonds and the thick dashed lines represent π–π stacking interactions.

Both crystal structures have slightly distorted tetrahedral coordination geometries with the Zn atoms. For compound **1**·CH_3CN, the bond lengths Zn1–Cl1, Zn1–Cl2, Zn1–N3, and Zn1–N4 are 2.235, 2.266, 2.022, and 2.031 Å, respectively. The bond angles around the Zn1 atom are in the range 107.9 to 112.1°. Compound **2**·CH_3CN has longer

 © 2008 Wiley-VCH Verlag GmbH & Co. KGaA, Weinheim

Zn1–I1 and Zn1–I2 bond lengths (2.582 and 2.604 Å) and similar Zn1–N3 and Zn1–N4 bond lengths (2.050 and 2.030 Å). The bond angles around the Zn1 atom in compound **2**·CH_3CN vary from 107.4 to 111.7°. The guest CH_3CN molecules are linked to compounds **1** and **2** by hydrogen bonds as shown in Table 2.

Table 2. Hydrogen-bond geometries for **1**·CH_3CN and **2**·CH_3CN.[a]

D–H···A	*d*(D···A) / Å	<(D–H···A) / °
1·CH_3CN		
N1–H1A···N5	2.314	161.0
N1–H1B···Cl2#	2.685	157.6
N3–H3C···Cl1#	2.777	133.5
2·CH_3CN		
N3–H3B···N5	2.312	156.2
N3–H3C···I2#	2.938	151.6
N1–H1B···I1#	3.007	135.7

[a] Symmetry code for **1**·CH_3CN and **2**·CH_3CN: # $x - 1, y, z$.

The molecular packings of compounds **1**·CH_3CN and **2**·CH_3CN extend in the linear direction, and the distances of the nearest Zn···Zn atoms are 5.021 and 5.153 Å, respectively. Hydrogen bonding and π–π stacking of the hybrid molecules are important for maintaining the 1D structures of compounds **1**·CH_3CN and **2**·CH_3CN (shown in Figure 2). Both interactions were affected by steric hindrance of the AEC ligand. The bond lengths and angles of Cl1($x - 1, y, z$)···H4B–N4 and Cl2($x - 1, y, z$)···H3B–N3 are not identical due to the distorted coordinate configuration of the Zn atom (as shown in Table 2). The π–π stacking in compounds **1** and **2** are parallel along the *a* axis. The closest interatom distances are C1···C4($x + 1, y, z$) and C3···C12($x + 1, y, z$) with distances of 3.545 and 3.619 Å for compounds **1** and **2**, respectively. The π–π stacking between the two carbazole rings on each side of the Zn atom are also different for compound **1**·CH_3CN (3.406 and 3.505 Å). The distances of the adjacent carbazole rings in compound **2**·CH_3CN are close to those of compound **1**·CH_3CN (3.340 and 3.530 Å), although the distances of the nearest Zn···Zn distances are larger in compound **2**·CH_3CN, which indicates that the π–π interactions are almost independent of the inorganic frameworks.

UV/Vis Spectroscopy

The UV/Vis spectra of AEC and the hybrid materials are shown in Figure 3. The structured peaks below 310 nm and a weak broad peak around 320–350 nm in AEC and compounds **1**–**4** are consistent with the absorption spectra of previously reported carbazole-containing compounds owning to the π→π* transition of the carbazole chromophore.[11] In the former report,[6] the energy gaps of the metal halide/organic N-donor ligand systems typically decrease according to the order Zn > Cd > Hg and Cl > Br > I as a result of the increasing ratio of the covalent/ionic bonding. However, the absorption spectra of compounds **1**–**4** are almost the same to that of AEC thin films (as shown in Figure 3). The energy gaps of AEC, $ZnCl_2(AEC)_2$, $ZnI_2(AEC)_2$, and $CdI_2(AEC)_2$ were determined to be 3.48, 3.46, 3.50, and 3.49 eV, which were obtained by the linear-fit process[12] of $(ahv)^2$ versus hv (a is the absorption coefficient). The energy gap of a thin film of $HgI_2(AEC)_2$ is a little smaller (3.41 eV, as shown in the inset of Figure 3), which may be due to the small energy gap of HgI_2.[13] These results indicate that the absorption of this type of hybrid material is correlated with the organic N-donor ligand rather than the inorganic metal halides. Comparison of the energy gaps of the metal halides $ZnCl_2$ (insulator), ZnI_2 (tetragonal, 4.05 eV), CdI_2 (polytype 4 H, 3.2 eV), and HgI_2 (tetragonal, 2.13 eV),[13] it can be concluded that the energy gaps of $ZnCl_2(AEC)_2$ and $ZnI_2(AEC)_2$ are much smaller than those of $ZnCl_2$ and ZnI_2.

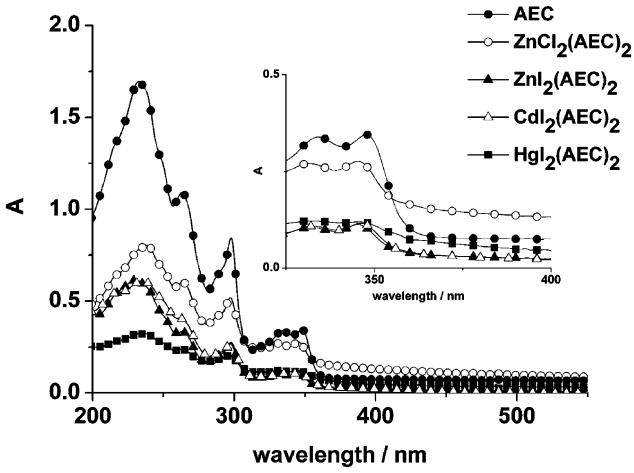

Figure 3. The UV/Vis spectra of the thin films of AEC (closed circles), $ZnCl_2(AEC)_2$ (open circles), $ZnI_2(AEC)_2$ (closed triangles), $CdI_2(AEC)_2$ (open triangles), and $HgI_2(AEC)_2$ (closed cubes). Inset: the absorption edge in the range 325–400 nm.

Photoluminescence Spectroscopy

The emission spectra of these compounds were carried out at room and liquid-nitrogen temperatures (as shown in Figure 4). At room temperature, the AEC spectrum consists of emissions centered at 377, 389, 416, and 437 nm (excited by 307 nm light), which are characteristic emission peaks for carbazole, and it also includes structured monomer fluorescence below 400 nm and broad excimer fluorescence in the range from 400 to 600 nm.[14] $ZnCl_2(AEC)_2$ has a strong emission with emission peaks centered at 372, 407, and 430 nm (excited by 310 nm light) at room temperature, which are very similar to the emission peaks of AEC. $ZnI_2(AEC)_2$ and $CdI_2(AEC)_2$ also have similar emission spectra with peaks centered at 370, 405, and 430 nm (both excited by 310 nm light) at room temperature, but the emission intensity from $CdI_2(AEC)_2$ is a little lower than that of $ZnI_2(AEC)_2$. In comparison to AEC, the $ZnCl_2(AEC)_2$, $ZnI_2(AEC)_2$, and $CdI_2(AEC)_2$ hybrid materials exhibit very weak emission at the wavelengths over 400 nm. This is because the emission from 410 to 440 nm for AEC is more

 © 2008 Wiley-VCH Verlag GmbH & Co. KGaA, Weinheim

likely to be quenched by the intramolecular heavy-atom effect.[15] Therefore, the AEC organic ligand gives blue emission, whereas $ZnCl_2(AEC)_2$, $ZnI_2(AEC)_2$, and $CdI_2(AEC)_2$ show deep-blue emissions. At liquid-nitrogen temperatures (77 K), AEC gives intensified excimer emission (over 400 nm), whereas $ZnCl_2(AEC)_2$, $ZnI_2(AEC)_2$, and $CdI_2(AEC)_2$ have a new emission peak at 356 nm, which is also from carbazole.[14] $HgI_2(AEC)_2$ is optically inert and no emission was detected at either room or liquid-nitrogen temperatures.

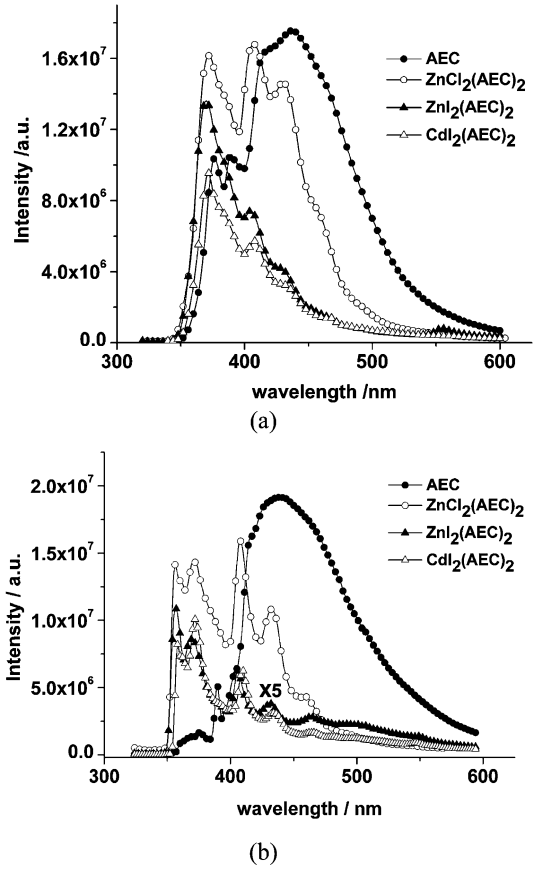

Figure 4. The photoluminescence spectra of AEC (closed circles), $ZnCl_2(AEC)_2$ (open circles), $ZnI_2(AEC)_2$ (closed triangles), and $CdI_2(AEC)_2$ (open triangles) in the solid state at room temperature (a) and at liquid-nitrogen temperature (b). Note that the intensities of the peaks in the spectra of $ZnI_2(AEC)_2$ and $CdI_2(AEC)_2$ were multiplied by a factor of five at low temperature.

The time-resolved radiative decays of AEC and compounds **1**–**3** were also measured (shown in Figure 5). The detected wavelengths are at 437 nm for AEC and 430 nm for $ZnCl_2(AEC)_2$, $ZnI_2(AEC)_2$, and $CdI_2(AEC)_2$. The decay curve of $ZnCl_2(AEC)_2$ is monoexponential with a lifetime of 18.64 ns, whereas the decay curves of AEC, $ZnI_2(AEC)_2$, and $CdI_2(AEC)_2$ are biexponential. The lifetime is 9.12 (46.54%) and 21.6 ns (53.46%) for AEC, 9.42 (77.23%) and 19.1 ns (22.77%) for $ZnI_2(AEC)_2$, and 4.10 (37.29%) and 8.58 ns (62.71%) for $CdI_2(AEC)_2$. The order of the lifetimes is $ZnCl_2(AEC)_2$ > AEC > $ZnI_2(AEC)_2$ > $CdI_2(AEC)_2$, which is indicative of the existence of the heavy-atom effect in $ZnI_2(AEC)_2$ and $CdI_2(AEC)_2$.[15] This result also indicates that the lack of luminescence of $HgI_2(AEC)_2$ is due to the heavy-atom effect of the Hg and I atoms.

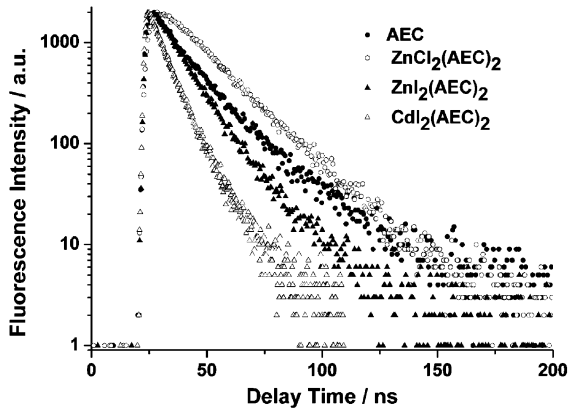

Figure 5. The photoluminescence spectra of AEC (closed circles), $ZnCl_2(AEC)_2$ (open circles), $ZnI_2(AEC)_2$ (closed triangles), and $CdI_2(AEC)_2$ (open triangles) in the solid state at room temperature (a) and at liquid nitrogen temperature (b).

In previous reports,[6] the mechanism of emission of metal halide/organic N-donor ligand hybrid systems was commonly attributed to charge-transfer processes, and apparently, the emission wavelengths changed with different metal halides. Only the $CdCl_2$/3,5-bis(pyrid-2-yl)-1,2,4-triazole system[16] was reported to have similar emission to that of the organic ligand, and the emission was assigned to intraligand fluorescence emission. Herein, compounds **1**–**3** also give emission similar to that of the AEC organic ligand. In order to explain the mechanism of emission, we carried out theoretical calculations on the electronic states of compounds **1** and **2** on the basis of their single-crystal structures (the guest CH_3CN molecules were omitted). The highest occupied molecular orbitals (HOMOs) and lowest unoccupied molecular orbitals (LUMOs) of compounds **1** and **2** are illustrated in Figure 6. It can be found clearly that the HOMOs and LUMOs of both compounds are mainly located on the carbazole rings of the AEC organic ligand, which is indicative of intraligand π–π* transition of the carbazole rings.[17] That is quite different from most other metal halide/organic N-donor ligand hybrids, in which the HOMOs are located on the halide atoms.[6,10]

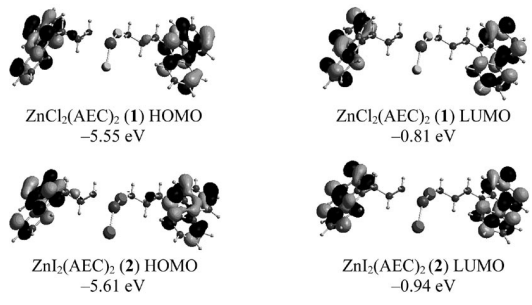

Figure 6. The surfaces of the frontier molecular orbitals of compounds **1** and **2** obtained at the B3LYP level. All the MO surfaces correspond to an isocontour value of $|\psi| = 0.03$ a.u.

 © 2008 Wiley-VCH Verlag GmbH & Co. KGaA, Weinheim

TD-DFT calculations were also employed to confirm the mechanism of emission (as shown in Table 3). Selected excited states with the greatest oscillator strengths of compounds **1** and **2** are designated to be the transition from the HOMO (or the degenerate energy level HOMO-1) to the LUMO, which is consistent with the absorption spectra. The calculated energy gaps of compounds **1** and **2** are also similar (4.10 and 4.03 eV), which are also in good agreement with the experimental energy gaps from the absorption spectra.

Table 3. Selected calculated excitation energies (*E*), oscillator strengths (*f*), and dominant excitation characteristics for low-lying singlet states for compounds **1** and **2**.

	State	Main contribution	$E_{calcd.}$ / eV	*f*
1	1	HOMO-1 → LUMO (0.46)	4.10	0.0507
	2	HOMO → LUMO (0.47)	4.10	0.0226
	6	HOMO-2→ LUMO (0.40)	4.56	0.2096
2	1	HOMO → LUMO (0.47)	4.03	0.0586
	2	HOMO-1 → LUMO (0.46)	4.03	0.0174
	3	HOMO → LUMO+2 (0.70)	4.41	0.0056

Conclusions

We synthesized and characterized the organic–inorganic hybrid materials $ZnCl_2(AEC)_2$ (**1**), $ZnI_2(AEC)_2$ (**2**), $CdI_2(AEC)_2$ (**3**), and $HgI_2(AEC)_2$ (**4**). This study has shown that the crystal structures of $ZnCl_2(AEC)_2{\cdot}CH_3CN$ (**1**·CH_3CN) and $ZnI_2(AEC)_2{\cdot}CH_3CN$ (**2**·CH_3CN) form quasi-1D structures by hydrogen bonding and π–π interactions. The distorted monomeric structures are due to the steric hindrance of the AEC ligand and the hydrogen bonding with the guest CH_3CN molecules. The energy gaps of this type of hybrid material are independent on the metal halides for $ZnCl_2(AEC)_2$ (**1**), $ZnI_2(AEC)_2$ (**2**), and $CdI_2(AEC)_2$ (**3**), whereas $HgI_2(AEC)_2$ (**4**) has a little smaller energy gap. The photoluminescence spectra, transient photoluminescence, and theoretical calculations prove that the emission of $ZnCl_2(AEC)_2$ (**1**), $ZnI_2(AEC)_2$ (**2**), and $CdI_2(AEC)_2$ (**3**) can be assigned to intraligand fluorescence emission mainly from the carbazole rings of the AEC ligand. $HgI_2(AEC)_2$ (**4**) is optically inert due to the strong quenching effect of the Hg and I atoms.

Experimental Section

Materials and Method: All chemicals are available from commercial sources and were used without further purification. $ZnCl_2$ (98%), ZnI_2 (99.5%), CdI_2 (99.5%), $HgCl_2$ (99%), KI (98.5%), sodium hydroxide (90%), and tetrabutylammonium bromide (99.0%) were purchased from Beijing Chemical Reagents Co.; carbazole (99.9%) was purchased from Tianjin Chemical Reagents Co.; and 2-chloroethylamine monohydrochloride (98%) was purchased from Acros Organics.

C, H, and N analyses were carried out with an Exeter Analytical CE-440 elemental analyzer. The infrared spectra (KBr pallet) were recorded with a Perkin–Elmer spectrum GX FTIR spectrophotometer. UV/Vis spectra were recorded with an Agilent 8453 spectrophotometer. Photoluminescence spectra were taken at room temperature (298 K) and liquid-nitrogen temperature (77 K) with a Jobin Yvon FluoroMax-3 spectrofluorometer with a xenon arc lamp as the light source. Time-resolved fluorescence decays were measured with a time-correlated single-photon counting (TCSPC) system on Edinburgh Instruments FLS920 and analyzed by the software provided by the supplier.

***N*-(2-Aminoethyl)carbazole (AEC):** The organic ligand was synthesized by following a literature procedure.[8] The product was purified by gradient-temperature sublimation. Yield: 66.2%. IR (KBr): $\tilde{\nu}$ = 3483 (w), 3284 (m), 3239 (m), 3140 (m), 3050 (m), 2947 (m), 2885 (s), 1595 (s), 1485 (s), 1454 (s), 1325 (s), 1004 (s), 745 (s), 724 (s), 642 (m) cm^{-1}. $C_{14}H_{14}N_2$ (210.27): calcd. C 79.97, H 6.71, N 13.32; found C 80.17, H 6.57, N 13.14.

$ZnCl_2(AEC)_2$ (1): A solution of $ZnCl_2$ (0.272 g, 0.002 mol) and AEC (0.840 g, 0.004 mol) in acetonitrile (60 mL) was stirred and heated at reflux for 1 h. The clear solution was then filtered and slowly cooled to room temperature. White-needle crystals of **1** (0.741 g, 66.6%) were obtained after drying in vacuo for 12 h. Slow evaporation of the filtrate over 7 d yielded colorless, cubic crystals that were suitable for X-ray measurement. IR (KBr): $\tilde{\nu}$ = 3287 (m), 3230 (m), 2940 (m), 2880 (m), 1572 (s), 1483 (s), 1453 (s), 1324 (s), 1238 (s), 988 (s), 747 (s), 722 (s), 640 (m) cm^{-1}. $C_{28}H_{28}Cl_2N_4Zn$ (556.84): calcd. C 60.39, H 5.07, N 10.06; found C 60.18, H 5.19, N 9.87.

$ZnI_2(AEC)_2$ (2): Compound **2** was synthesized by following a procedure similar to that of compound **1**. Yield: 67.6%. Slow evaporation of the filtrate over 3 d yielded colorless, cubic crystals that were suitable for X-ray measurement. IR (KBr): $\tilde{\nu}$ = 3557 (w), 3302 (m), 3235 (m), 3047 (m), 2935 (m), 1580 (s), 1484 (s), 1454 (s), 1325 (s), 1230 (m), 1008 (m), 745 (s), 723 (m) cm^{-1}. $C_{28}H_{28}I_2N_4Zn$ (739.75): calcd. C 45.46, H 3.82, N 7.57; found C 45.48, H 3.77, N 7.56.

$CdI_2(AEC)_2$ (3): Compound **3** was synthesized by following a procedure similar to that of compound **1**. Yield: 69.9%. IR (KBr): $\tilde{\nu}$ = 3524 (w), 3309 (m), 3245 (m), 3048 (w), 2936 (m), 1593 (m), 1484 (s), 1453 (s), 1325 (s), 1238 (s), 983 (m), 745 (s), 722 (s) cm^{-1}. $CdI_2C_{28}H_{28}N_4$ (786.77): calcd. C 42.74, H 3.59, N 7.12; found C 42.53, H 3.47, N 7.07.

$HgI_2(AEC)_2$ (4): HgI_2 was obtained by mixing water solutions of $HgCl_2$ and KI. HgI_2 was then purified by recrystallization (2×) from ethanol. Compound **4** was synthesized by following a procedure similar to that of compound **1**. Yield: 60.7%. IR (KBr): $\tilde{\nu}$ = 3417 (m), 3320 (m), 3260 (m), 3049 (m), 2922 (m), 1594 (m), 1485 (s), 1451 (s), 1326 (s), 747 (s), 722 (s) cm^{-1}. $HgI_2C_{28}H_{28}N_4$ (874.95): calcd. C 38.44, H 3.23, N 6.40; found C 38.24, H 3.40, N 6.23.

Calculation Details: Calculations on the ground and excited electronic states of compounds **1** and **2** were carried out by using density functional theory (DFT) and time-dependent DFT (TD-DFT) at the B3LYP level.[18] "Double-ξ" quality basis sets were employed for the C, H, and N (6-31G*) atoms and the Zn, Cd, Hg, Cl, I (LANL2DZ) atoms. The initial ground-state geometries were directly obtained from the X-ray crystal structures. The geometries were fully optimized with C_1 symmetry constraints. All calculations were performed with the Gaussian 03 software package by using a spin-restricted formalism.[19] The electron density diagrams of the molecular orbitals were obtained with the ChemOffice 2002 graphics program.

X-ray Crystallography: Crystals of compounds **1**·CH_3CN and **2**·CH_3CN with the same dimensions of 0.4 × 0.1 × 0.05 mm were

 © 2008 Wiley-VCH Verlag GmbH & Co. KGaA, Weinheim

selected under a microscope and attached to the end of a quartz fiber. The room temperature (294 ± 1 K) single-crystal X-ray experiments were performed with a Bruker P4 diffractometer equipped with graphite-monochromatized Mo-K_α radiation (λ = 0.710 73 Å) by using the ω scan technique. Direct phase determination yielded the positions of the Zn, Cl, I, N, and most of the C atoms. The remaining atoms were located in successive-difference Fourier syntheses. Hydrogen atoms were generated theoretically and rode on their parent atoms in the final refinement. All non-hydrogen atoms were subjected to anisotropic refinement. The structural solutions and refinements were performed by using the SHELXTL NT v 5.10 program package (Bruker, 1997).[20] A summary of the refinement details and the resulting factors are given in Table 4.

Table 4. Crystallographic data for **1**·CH_3CN and **2**·CH_3CN.

Parameters	**1**·CH_3CN	**2**·CH_3CN
Empirical formula	$C_{30}H_{31}N_5ZnCl_2$	$C_{30}H_{31}N_5ZnI_2$
Molecular mass	597.87	780.77
Color	colorless	colorless
Crystal system	monoclinic	monoclinic
Space group	$P2_1/n$	$P2_1/n$
a / Å	5.021 (1)	5.153 (1)
b / Å	15.425 (3)	15.955 (3)
c / Å	37.902 (8)	37.609 (8)
β / °	92.20 (3)	92.16 (3)
V / Å^3	2933.3 (1)	3089.9 (1)
Z	4	4
$D_{calcd.}$ / g cm^{-3}	1.354	1.678
Absorp. coeff. (μ) / mm^{-1}	1.047	2.820
R_1, wR_2 [I ≧ 2σ(I)][a]	0.0615, 0.1272	0.0444, 0.1000
R_1, wR_2 (all data)[a]	0.1461, 0.1556	0.0599, 0.1068

[a] $R_1 = \Sigma||F_o|-|F_c||/\Sigma|F_o|$; $wR_2 = [\Sigma w(F_o^2 - F_c^2)^2/\Sigma(F_o^2)^2]^{1/2}$.

CCDC-673277 (for **1**·CH_3CN) and -673278 (for **2**·CH_3CN) contain the crystallographic data for this paper. These data can be obtained free of charge from The Cambridge Crystallographic Data Centre via www.ccdc.cam.ac.uk/data_request/cif.

Acknowledgments

This work was supported by the National Natural Science Foundation of China (No. 50433020 and 50403001) and the National Basic Research Program of China (No. 2006CB806200). Thanks to Prof. Yongge Wei in the Department of Chemistry at Tsinghua University for solving the X-ray data.

[1] a) R. D. Bailey, L. L. Hook, A. K. Power, T. W. Hanks, W. T. Penningtou, *Cryst. Eng.* **1998**, *1*, 51–66; b) P. M. Graham, R. D. Pike, M. Sabat, R. D. Bailey, W. T. Pennington, *Inorg. Chem.* **2000**, *39*, 5121–5132; c) J. H. Yu, L. Ye, M. H. Bi, Q. Hou, X. Zhang, J. Q. Xu, *Inorg. Chim. Acta* **2007**, *360*, 1987–1994.

[2] Y. Song, Y. Niu, H. Hou, Y. Zhu, *J. Mol. Struct.* **2004**, *689*, 69–74.

[3] a) J. Ni, Y. Xie, X. Liu, Q. Liu, *Appl. Organomet. Chem.* **2003**, *17*, 315–316; b) R. D. Bailey, W. T. Pennington, *Polyhedron* **1997**, *16*, 417–422.

[4] W. T. Chen, X. N. Fang, Q. Y. Luo, Y. P. Xu, Y. P. Duan, *Acta Crystallogr., Sect. C* **2007**, *63*, m398–400.

[5] a) D. A. Handley, P. B. Hitchcock, T. H. Lee, G. J. Leigh, *Inorg. Chim. Acta* **2001**, *314*, 14–21; b) A. Altun, K. Gölcük, M. Kumru, *Vib. Spectrosc.* **2003**, *33*, 63–74; c) J. H. Yu, Q. Hou, T. G. Wang, X. Zhang, J. Q. Xu, *J. Solid State Chem.* **2007**, *180*, 518–522.

[6] W. T. Chen, M. S. Wang, X. Liu, G. C. Guo, J. S. Huang, *Cryst. Growth Des.* **2006**, *6*, 2289–2300.

[7] K. R. J. Thomas, J. T. Lin, Y. T. Tao, C. W. Ko, *Adv. Mater.* **2000**, *12*, 1949–1951.

[8] A. M. Cuadro, M. P. Matia, J. L. Garcia, J. J. Vaquero, J. Alvarez-Builla, *Synth. Commun.* **1991**, *21*, 535–544.

[9] C. Hu, Q. Li, U. Englert, *CrystEngComm* **2003**, *5*, 519–529.

[10] B. Xiao, H. Hou, Y. Fan, M. Tang, *Inorg. Chem. Commun.* **2007**, *10*, 376–380.

[11] M. Deng, G. Wo, S. Y. Cheng, M. Wang, G. Borgrs, H. Z. Chen, *Mater. Sci. Eng. B* **2008**, *147*, 90–94.

[12] D. Ramirez, D. Silva, H. Gomez, G. Riveros, R. E. Marotti, E. A. Dalchiele, *Sol Energy Mater. Sol Cells* **2007**, *91*, 1458–1461.

[13] P. Tyagi, A. G. Vedeshwar, *Phys. Rev. B* **2001**, *64*, 245406.

[14] P. Mandal, T. Misra, A. De, S. Ghosh, S. R. Chaudhury, J. Chowdhury, T. Ganguly, *Spectrochim. Acta A* **2007**, *66*, 534–545.

[15] S. M. Bonesi, R. Erra-Balsells, *J. Lumin.* **2002**, *97*, 83–101.

[16] Q. G. Zhai, X. Y. Wu, S. M. Chen, C. Z. Lu, W. B. Yang, *Cryst. Growth Des.* **2006**, *6*, 2126–2135.

[17] B. Liu, X. C. Zhang, Y. F. Wang, *Inorg. Chem. Commun.* **2007**, *10*, 199–203.

[18] a) A. D. Becke, *J. Chem. Phys.* **1993**, *98*, 5648–5652; b) C. Lee, W. Yang, R. G. Parr, *Phys. Rev. B* **1988**, *37*, 785–789.

[19] M. J. Frisch, G. W. Trucks, H. B. Schlegel, G. E. Scuseria, M. A. Robb, J. R. Cheeseman, J. A. Montgomery Jr., T. Vreven, K. N. Kudin, J. C. Burant, J. M. Millam, S. S. Iyengar, J. Tomasi, V. Barone, B. Mennucci, M. Cossi, G. Scalmani, N. Rega, G. A. Petersson, H. Nakatsuji, M. Hada, M. Ehara, K. Toyota, R. Fukuda, J. Hasegawa, M. Ishida, T. Nakajima, Y. Honda, O. Kitao, H. Nakai, M. Klene, X. Li, J. E. Knox, H. P. Hratchian, J. B. Cross, C. Adamo, J. Jaramillo, R. Gomperts, R. E. Stratmann, O. Yazyev, A. J. Austin, R. Cammi, C. Pomelli, J. W. Ochterski, P. Y. Ayala, K. Morokuma, G. A. Voth, P. Salvador, J. J. Dannenberg, V. G. Zakrzewski, S. Dapprich, A. D. Daniels, M. C. Strain, O. Farkas, D. K. Malick, A. D. Rabuck, K. Raghavachari, J. B. Foresman, J. V. Ortiz, Q. Cui, A. G. Baboul, S. Clifford, J. Cioslowski, B. B. Stefanov, G. Liu, A. Liashenko, P. Piskorz, I. Komaromi, R. L. Martin, D. J. Fox, T. Keith, M. A. Al-Laham, C. Y. Peng, A. Nanayakkara, M. Challacombe, P. M. W. Gill, B. Johnson, W. Chen, M. W. Wong, C. Gonzalez, J. A. Pople, *Gaussian 03*, Revision B.03, Gaussian, Inc., Pittsburgh PA, **2003**.

[20] G. M. Sheldrick, *SHELXTL*, version 5.1, Bruker Analytical X-ray System, Madison WI, **1997**.

Received: January 22, 2008
Published Online: May 20, 2008

 © 2008 Wiley-VCH Verlag GmbH & Co. KGaA, Weinheim